LRP 468/92 December 1992

PRESSURE AND INDUCTANCE EFFECTS ON VERTICAL STABILITY OF SHAPED TOKAMAKS

D.J. Ward, A. Bondeson and
F. Hofmann

submitted for publication in
NUCLEAR FUSION, Letters

PRESSURE AND INDUCTANCE EFFECTS ON VERTICAL STABILITY OF SHAPED TOKAMAKS

D.J. Ward, A. Bondeson, F. Hofmann
Centre de Recherches en Physique des Plasmas,
Association Euratom–Confédération Suisse,
Ecole Polytechnique Fédérale de Lausanne,
21 av. des Bains, 1007 Lausanne, Switzerland

Abstract

Numerical calculations are presented to show the influence of finite pressure on the vertical stability of shaped tokamaks. High $\epsilon\beta_p$ improves the vertical stability of dee-shaped tokamaks but is destabilizing for an inverse dee. For highly elongated cross sections, the pressure effect is well described by a linear dependence of the maximum value of stable internal inductance on $\epsilon\beta_p$, with a coefficient that depends on the geometry and increases with triangularity. Stability diagrams are shown in terms of $l_{i,crit}$ versus $\epsilon\beta_p$ for TCV- and DIII-D-like cross sections. The effects of pressure are significant even in the absence of a surrounding wall. Current profile effects depend critically on the wall configuration: low values of l_i increase the driving force of the instability, but are stabilizing if the wall is sufficiently close.

1. Introduction

Modern tokamaks are generally designed so as to take advantage of the increased current capability of an elongated cross section and the resulting improvement of the beta limit [1,2] and confinement time [3]. A well-known drawback of elongation is vertical instability [4,5], and for sufficiently high elongation, this requires the use of conducting walls close to the plasma assisted by active feedback stabilization on the L/R time-scale of the resistive wall. Work on the DIII-D tokamak has established that vertical instability is the factor which limits the achievable elongation [2,6]. For the TCV experiment [7] in Lausanne, designed for a maximum elongation of $\kappa = 3$, the vertical stability is a main issue, and we have therefore investigated numerically the operational limits due to the vertical instability and how these depend on, e.g., the shape of the plasma cross section and the equilibrium profiles.

It is well known [8] that vertical stability of strongly elongated tokamaks is favored by a low internal inductance l_i, because this increases the coupling of the plasma current to the external conductors. Thus vertical stability requires an internal inductance less than some threshold $l_{i,crit}$, which decreases with increasing elongation and wall distance. Here, we mean by $l_{i,crit}$ the value of l_i for which an equilibrium surrounded by a realistic resistive wall has a growth rate γ_{crit}, below which the vertical position can be controlled by a practical feedback system.

Our principal result is that $l_{i,crit}$ is strongly influenced by pressure in combination with triangular shaping of the cross section. We find numerically that $l_{i,crit}$ is an approximately linear function of $\epsilon\beta_p$, independent of details of the current profile and aspect ratio, but sensitively dependent on the geometry of the cross section and the wall distance. For the usual dee shape, pressure is stabilizing, i.e., $l_{i,crit}$ increases with $\epsilon\beta_p$, whereas in an inverse dee, pressure is destabilizing. The increased upper limit in internal inductance for a normal dee is a favorable effect, not only because it makes it possible to reach a higher

elongation, but also because the beta limit [2,9] and confinement time [10] improve with the internal inductance at fixed elongation. Reference [2] shows convincing evidence that the optimum condition for reaching high beta is at the intersection of the $n = 0$ and $n = 1$ stability boundaries.

2. Stability Diagrams for TCV and DIII-D Cross Sections

Figure 1 shows the limit in internal inductance $l_{i,crit}$ as a function of $\epsilon\beta_p$ for three different classes of current profiles in a "TCV cross section" at aspect ratio $A = 1/\epsilon = R_0/a = 3.7$ (curves 1 – 3). The following definitions are used for the poloidal beta, $\beta_p \equiv (4/\mu_0 I_p^2 R_0) \int_{pl} p d^3x$, and internal inductance, $l_i \equiv (2/\mu_0^2 I_p^2 R_0) \int_{pl} B_p^2 d^3x$. The plasma-vacuum boundary is specified as

$$R/a = A + \cos(\theta + \delta \sin\theta + \lambda \sin 2\theta) \quad , \quad Z/a = \kappa \sin\theta \tag{1}$$

and the geometry referred to as "TCV cross section" has elongation $\kappa = 3$, triangularity $\delta = 0.5$ and squareness $\lambda = 0.2$. Equilibria have been computed with the CHEASE code [11] and stability with the NOVA-W code [12], which is capable of computing growth rates of $n = 0$ modes with a resistive wall, as well as with an ideal wall or no wall. Figure 1 refers to resistive wall instabilities (cases stable with an ideal wall), and it is assumed that the mode can be stabilized by feedback if the resistive wall growth time is longer than 7% of the L/R time of the wall (more precisely, for its "m = 1" eigenmode). The conducting wall has been chosen to represent the TCV vacuum vessel [7].

Several conclusions can be drawn from Fig. 1. First, the limit in l_i is the same function of β_p for the three different classes of current profiles. The three current profiles differ significantly, and Fig. 2 shows the profiles 1 and 3 for the surface averaged toroidal current density I* at the point $l_i = l_{i,crit}$ at low and high pressure ($\epsilon\beta_p = 0$ and 0.5 respectively). (The pressure profiles have been chosen as uniformly scaled versions of those that give the ballooning limit with a given I* profile.) Secondly, curve 4 refers to an equilibrium with

larger aspect ratio, $A = 7$. The large aspect ratio result coincides almost exactly with those for $A = 3.7$ when plotted in terms of l_i and $\epsilon\beta_p$. Thus, for a fixed, elongated cross section (but varying the current profile and the aspect ratio), $n = 0$ stability requires $l_i < l_{i,crit}(\epsilon\beta_p)$ and for $\epsilon\beta_p$ not too large, $l_{i,crit}$ is almost linear in $\epsilon\beta_p$; $l_{i,crit} \approx l_{i,0} + c\,\epsilon\beta_p$, where c may depend on the geometry.

Figure 3 shows the corresponding result for a DIII-D-like cross section, $\kappa = 2.5$, $\delta = 0.6$, $\lambda = 0$ and $A = 3$. Here, the resistive wall was chosen to be conformal to the plasma boundary, and two different minor radii have been considered for the wall; $d = 1.3a$ and $d = 1.4a$. The result is similar to that for TCV in that the critical internal inductance increases with $\epsilon\beta_p$, however, the dependence is much stronger for the DIII-D cross section. For the DIII-D-like case with $d = 1.3a$, we have $l_{i,crit} \approx l_{i,0} + c\,\epsilon\beta_p$, with $c \approx 1.8$, which is much larger than for the TCV cross section, where $c \approx 0.34$.

The stability threshold of course depends on the assumptions concerning the critical growth rate γ_{crit}. If the critical growth rate is changed, the main effect is on the value of $l_{i,crit}$ with only a small effect on the value of the slope c. For example, if γ_{crit} for the TCV case, Fig. 1, is increased by 50% (this relaxes the demands on the feedback system), then the value of $l_{i,0}$ increases from 0.494 to 0.519, while the slope c increases by about 8%. For the DIII-D-like case, if γ_{crit} is increased by 50% the value of $l_{i,0}$ increases considerably from 0.521 to 0.667, but the value of the slope c increases by only 3%.

Note that Fig. 3 does not apply literally to DIII-D conditions, e.g., with respect to the assumed value of $\gamma_{crit} \cdot \tau_{wall}$. Furthermore, our definitions of β_p and l_i differ from those used in e.g. Ref. [2] by a shape dependent factor. For the DIII-D shape our values are smaller by a factor ≈ 1.5.

3. Brief Review of Theoretical Results

Several results relevant to the diagrams in Figs. 1 and 3 have been obtained previously by analytic [4,5,13,14,16], semi-analytic [17,18] or numerical [19,20] methods. Quite surprisingly, most of the work on shape, pressure, and inductance effects on vertical stability dates from the seventies, despite the subsequent development of powerful numerical codes and the fact that experiments are now in regimes where such effects are of importance.

Zakharov [4] showed that vertical elongation, $\kappa > 1$, destabilizes vertical shifts but that a weakly elongated equilibrium can be stabilized by finite aspect ratio effects without the use of a conducting shell. Vertical displacements are stable if the decay index n of the external vertical field satisfies $n \equiv -(R_0/B_z^{\rm ext})(\partial B_z^{\rm ext}/\partial R)_{R=R_0} > 0$.

Zakharov's [4,5] expression for n implies that a plasma with a flat current profile is stable when

$$\kappa - 1 < \left(\frac{a}{R_0}\right)^2 \left(\frac{3}{4}\log\frac{8R_0}{a} - \frac{17}{16}\right). \tag{2}$$

Laval et al. [13] showed that an elongated plasma can be stabilized by a conducting wall. For a flat current profile, their stability condition (in the near circular approximation) reads

$$\kappa - 1 < 2\left(\frac{a}{d}\right)^2, \tag{3}$$

where d is the wall radius. Comparison of the conditions (2) and (3) shows that for elongations, aspect ratios and wall distances typical of modern tokamaks, wall stabilization is far more important than finite aspect ratio effects [21], and the discharges would be strongly unstable without a wall.

Effects of more complex shaping, including finite aspect ratio and pressure effects, were investigated semi-analytically for a surface current distribution by Rebhan and Salat [18]. For vertically elongated equilibria, they found that an inverse dee ($\delta < 0$) is destabilized by pressure, but a standard dee ($\delta > 0$) can be stabilized by pressure (see Fig. 4a of Ref. [18]). A stabilizing effect of finite pressure in combination with positive triangularity

on the vertical stability of elongated equilibria is also indicated by results [19] obtained with the ERATO stability code. This effect is the basic reason for the increased $l_{i,crit}$ at high $\epsilon\beta_p$ in the operational diagrams, Figs. 1 and 3. The main new result shown in these diagrams is the appreciable size of the pressure effect on vertical stability in terms of operational parameters, l_i and $\epsilon\beta_p$, for more realistic current distributions than the surface current model of Ref. [18].

It has been shown [14,15] that resistive wall growth rates (for equilibria that are unstable without any wall but stable with an ideally conducting wall) can be expressed in terms of the ideal-MHD potential energies of the vertical shift mode in the absence of a wall, δW_∞, and with an ideally conducting wall in the position of the resistive wall, δW_d, as $\gamma_{res} = -(b/\tau_w)\delta W_\infty/\delta W_d$. Here, τ_w is the L/R time of the wall and b is a numerical factor that depends on the current distribution in the wall. This expression gives valuable analytical insight. However, for numerical calculations it is more straightforward to introduce an actual resistive wall and solve the full eigenvalue problem as is done by NOVA-W. This automatically takes into account the effects of non-rigid shifts [22] and avoids the calculation of δW_d for a stable oscillatory mode which can be hidden by a continuous spectrum.

In the following two sections, we show vertical stability results for ideal and resistive walls obtained with the NOVA-W code with the aim of placing the results for TCV and DIII-D cross sections into a broader framework.

4. Pressure Effects

The operational diagrams in Figs. 1 and 3 show a much stronger stabilizing effect of $\epsilon\beta_p$ in the DIII-D-like cross section ($\kappa = 2.5$, $\delta = 0.6$, $\lambda = 0$) than for TCV shape ($\kappa = 3.0$, $\delta = 0.5$, $\lambda = 0.2$). It appears that the most important reason for this difference is the more triangular shape of DIII-D (note that a positive λ decreases the effective triangularity [9]).

The strong dependence of the pressure effect on triangularity is illustrated by Fig. 4. This figure shows resistive wall growth rates for elongated cross sections ($\kappa = 2.5$, $A = 3$) at low and high pressure ($\beta_p = 0.06$ and 0.6, respectively) and three different triangularities $\delta = -0.6$ (inverse dee), 0.0 (ellipse), and +0.6 (standard dee). The wall is a conformal copy of the plasma surface with minor radius $d = 1.3a$ and has the same resistivity and thickness as the TCV vacuum vessel used for Fig. 1. Figure 4 shows that the pressure is strongly destabilizing for the inverse dee, somewhat stabilizing for the ellipse, and clearly stabilizing for the standard dee. The inverse dee is strongly destabilized, and with $\beta_p = 0.6$ the mode is near marginal stability with an ideally conducting wall, see Eq. (3).

Figure 5 shows the square of the ideal-wall growth rate (a measure of the ideal-MHD driving energy) vs. the reciprocal wall radius squared for the different triangularities and pressures. The three points shown for each of the six curves correspond to the wall at infinity, at $d = 1.6a$, and at the critical ideal wall distance to stabilize the axisymmetric mode. The dee shape is clearly the most stable among all cases (see also Fig. 4), and for this configuration finite pressure is significantly stabilizing in the absence of a wall, and remains so when wall stabilization is accounted for.

By contrast, for the inverse dee pressure is clearly destabilizing both with and without a wall. The critical wall distance for the inverse dee is quite close to $d = 1.3a$, and therefore the resistive wall growth rate (with the wall at that position) is quite high in Fig. 4 for that case. For the pure ellipse, the free space growth rate is virtually the same for the low and high pressure cases, but high pressure shows a stabilizing influence in the presence of a wall, and the growth rate falls below that for the inverse dee as the wall is moved inward.

We can see from plots of the equilibrium flux surfaces that, for the dee shape, increased pressure reduces the central elongation. This can be interpreted as the result of squeezing in the vertical direction by the combination of triangular shape and the Shafranov shift.

The same effect leads to an increased elongation at high β_p in an inverse dee.

Therefore we see that the primary effect of pressure on the dee shape is to lower the free space driving energy, while it increases the free space energy for the inverse dee. Thus the favorable effect of pressure shown in the operational diagrams, Figs. 1 and 3, is mainly due to lowering the free space driving energy and not to the wall coupling. For the ellipse, the free space growth rates are virtually unaffected by pressure, but there is an increase in the wall stabilization for the high pressure case.

5. Current Profile Effects

It is well known that the peaking of the current profile can have significant effects on the vertical stability. The good agreement between the curves for different classes of current profiles in Fig. 1 shows that the relevant parameter characterizing the current distribution is the internal inductance. Flat current profiles with low internal inductance lead to stronger coupling between the plasma and the external conductors. (Stated differently, the poloidal field, and hence the flux perturbation due to a rigid displacement, become larger in the external region when the internal inductance is low.) However, we find that, in the absence of a conducting shell, the growth rate generally increases with decreasing inductance (see also Ref. [20]). This is shown in Fig. 6, where the ideal wall growth rate is plotted as a function of the wall radius for two DIII-D-shaped equilibria with different internal inductance $l_i = 0.6$ and 0.8, respectively.

Peaking of the current profile is evidently stabilizing when the wall is distant but destabilizing when the wall is sufficiently close. At a wall distance of roughly $d = 1.4a$, the two curves in Fig. 6 cross, and the growth rate is independent of the inductance. This point is close to the critical wall distance. Therefore, the internal inductance may have a rather small effect on the ideally marginal wall position, but it may have a much stronger effect on the resistive growth rates [14]. In fact, with the wall at $d = 1.3a$,

the two cases in Fig. 6 have nearly a factor of 2 difference in the resistive growth rate. Figure 3 shows that the β_p required to stabilize equilibria with these two inductances increases from 0.13 at $l_i \approx 0.6$ to 0.46 at $l_i \approx 0.8$. The reduction of the free space growth rate with increasing inductance appears to be due mainly to a reduction of the ellipticity of the central flux surfaces. It should be noted that there are many competing effects, for example a similar reduction of the central triangularity, which reduces the finite pressure stabilization. In addition, peaking of the current profile effectively increases the aspect ratio, so that the toroidal stabilization is reduced. However, as discussed in Sec. 3, the toroidal stabilization is not very significant for highly elongated cross sections.

5.1. Passive Stabilization by Discrete Conductors

While the effect of broadening the current profile increases the destabilizing force on the equilibrium, it also increases the stabilizing effect of a completely surrounding conducting wall. The balance between these competing effects would clearly be changed if the passive stabilization is provided primarily by discrete sets of nearby conductors instead of a surrounding wall. We consider a configuration in which the vacuum vessel is far from the plasma, and the plasma is passively stabilized by a close set of conductors on the outboard side and another set on the inboard side. The equilibrium has $\kappa = 1.9$, $\delta = 0.7$, and $A = 4.54$. Figure 7 shows that in this configuration the growth rate increases with decreasing l_i. This effect has been observed previously by Pearlstein [23] and Jardin [24].

As a comparison we do the calculation with a resistive wall conformal to the plasma shape at $d = 1.3a$ with the total wall resistance normalized to that of the passive conductors of this configuration. We see from Fig. 7 that with the closed-wall configuration the growth rate decreases monotonically with decreasing l_i.

Figure 8 shows the plasma boundary, the discrete sets of conductors, the distant

vacuum vessel wall, and the fictitious wall used in Fig. 7 (the latter is shown as a dotted contour). Figure 8 also shows the contours of perturbed flux for the high l_i case (a) and the low l_i case (b) in this configuration. These plots show that the coupling of the perturbed flux to the conductors is not very good in the low l_i case. Therefore the increase in the destabilizing force due to the broader current profile dominates, and the growth rate increases with decreasing l_i.

We conclude that for highly elongated tokamaks, there are two main effects of the internal inductance on vertical stability. First of all, wall stabilization is improved for low internal inductance because of increased magnetic coupling. Second, current peaking reduces the shaping of the internal flux surfaces which reduces the instability growth rate in the absence of a wall. For highly elongated, feedback stabilized discharges with a closed wall, the effect on wall coupling is the more important, and stability improves at low inductance. However, the competition of these two effects is more subtle when there is not a completely surrounding wall, and depends on the details of the current profile and the placement of the nearby conductors.

6. Conclusion

We have found that high $\epsilon\beta_p$ significantly improves the vertical stability of elongated, dee-shaped tokamaks. Our results for the TCV cross section indicate that the effect can be described in terms of an almost linear dependence of the critical internal inductance on $\epsilon\beta_p$, $l_{i,crit} \approx l_{i,0} + c\,\epsilon\beta_p$. Comparison between different cross sections shows that the coefficient c increases with the triangularity, and the dependence of $l_{i,crit}$ on $\epsilon\beta_p$ is quite pronounced for a DIII-D cross section. This effect is beneficial for reaching high beta because it increases the maximum stable elongation or, alternatively, allows the current profile to be more peaked which increases the beta limit due to the $n = 1$ external kink mode [2,9].

Acknowledgments

This work was supported in part by the Swiss National Science Foundation. We acknowledge the work of Dr. H. Lütjens in adapting the CHEASE equilibrium code for NOVA-W.

REFERENCES

[1] TROYON, F., GRUBER, R., SAURENMANN, H., SEMENZATO, S., SUCCI, S., Plasma Phys. Contr. Fusion **26** (1984) 209.

[2] LAZARUS, E. A., CHU, M. S., FERRON, J. R., et al., Phys. Fluids **B3** (1991) 2220; LAZARUS, E.A., LAO, L.L., OSBORNE, T.H., et al., Phys. Fluids **B4** (1992) 3644.

[3] YUSHMANOV, P.N., TAKIZUKA, T., RIEDEL, K.S., et al., Nucl. Fusion **30** (1990) 1999.

[4] ZAKHAROV, L.E., Sov. Phys. - Tech. Phys. **16** (1971) 645 [Zh. Tekh. Fiz. **41** (1971) 823].

[5] MUKHOVATOV,V.S., SHAFRANOV, V.D., Nucl. Fusion **11** (1971) 605.

[6] LAZARUS, E. A., LISTER, J. B., NEILSON, G .H., Nucl. Fusion, **30** (1990) 111.

[7] HOFMANN, F., JARDIN, S. C., MARCUS, F. B, PEREZ, A., TURNBULL, A. D., in Fusion Technology (Proc. 14th Symp. Avignon, 1986), Vol. 1, Pergamon Press, Oxford (1986) 687.

[8] TAYLOR, T.S., LAZARUS, E.A., CHU, M.S., et al., in Plasma Physics and Controlled Nuclear Fusion Research 1990 (Proc. 13th Int. Conf. Washington, D.C., 1990), Vol. 1, IAEA Vienna (1991), 177; LAO, L.L., TAYLOR, T. S., CHU, M. S., et al., Phys. Fluids **B4** (1992) 232.

[9] ERIKSSON, G., BONDESON, A., WARD, D.J., HOFMANN, F., VILLARD, L., in Proc. 1992 Int. Conf. on Plasma Phys., Vol. 16C, part I, European Physical Society (1992) 343.

[10] ZARNSTORFF, M.C., BARNES, C.W., EFTHIMION, P.C., et al., in Plasma Physics and Controlled Nuclear Fusion Research 1990 (Proc. 13th Int. Conf. Washington, D.C., 1990), Vol. 1, IAEA Vienna (1991), 109.

[11] LÜTJENS, H., BONDESON, A., ROY, A., Comput. Phys. Comm. **69** (1992) 287.

[12] WARD, D. J., JARDIN, S. C., CHENG, C. Z., Calculation of Axisymmetric Stability of Tokamak Plasmas with Active and Passive Feedback, Report PPPL-2776, Princeton University Plasma Physics Laboratory (July 1991). To appear in J. Comput. Phys. **104** (1993).

[13] LAVAL, G., PELLAT, R., SOULÉ, J.S., Phys. Fluids **17** (1974) 835.

[14] HANEY, S.W., FREIDBERG, J.P., Phys. Fluids **B1** (1989) 1637.

[15] Hofmann, F., Schultz, C. G., in Controlled Fusion and Plasma Physics (Proc. 11th Eur. Conf. Venice, 1989), Vol. 13B Part I, European Physical Society (1987) 335.

[16] ERIKSSON, H. G., Plasma Phys. Control. Fusion, **34** (1992) 1721.

[17] REBHAN, E., Nucl. Fusion **15** (1975) 277.

[18] REBHAN, E., SALAT, A., Nucl. Fusion **16** (1976) 805.

[19] BERNARD, L.C., BERGER, D., GRUBER, R., TROYON, F., Nucl. Fusion **18** (1978) 1331.

[20] BECKER, G., LACKNER, K., in Plasma Physics and Controlled Nuclear Fusion Research 1976 (Proc. 6th Int. Conf. Berchtesgaden, 1976), Vol. 2, IAEA Vienna (1977), 401.

[21] STAMBAUGH, R.D., LAO, L.L., LAZARUS, E.A., Nucl. Fusion, **32** (1992) 1642.

[22] WARD, D. J., JARDIN, S. C., Nucl. Fusion **32** (1992) 973.

[23] PEARLSTEIN, L. D., personal communication.

[24] JARDIN, S. C., personal communication.

Figures

Fig. 1. Vertical stability diagram in terms of l_i and $\epsilon\beta_p$ for the TCV configuration. Curves 1–3 show the results for the standard TCV configuration for 3 different types of current profiles. Curve 4 shows results for the TCV plasma and wall shape expanded to an aspect ratio of $R_0/a = 7.0$ for the first current profile.

Fig. 2. Current profiles corresponding to curves 1 and 3 of Fig. 1. Both profile types are shown at low and high beta: (a) curve 1, $\beta_p = 0.06$; (b) curve 1, $\beta_p = 0.6$; (c) curve 3, $\beta_p = 0.06$; (d) curve 3, $\beta_p = 0.6$.

Fig. 3. Vertical stability diagram in terms of l_i and $\epsilon\beta_p$ for the DIII-D-like equilibrium. The two curves are for two different wall positions. The walls are conformal to the plasma shape at a midplane distance of $d = 1.3a$ and $d = 1.4a$. Also shown, for comparison, is curve 1 from Fig. 1 for the TCV configuration.

Fig. 4. Growth rates (in s^{-1}) vs. triangularity for a resistive wall conformal to the plasma shape at a midplane distance of $d = 1.3a$ for three shapes: the inverse dee, ellipse, and regular dee ($\delta = -0.6, 0.0, 0.6$, respectively) at high beta ($\beta_p = 0.6$) and low beta ($\beta_p = 0.06$).

Fig. 5. Plot of γ^2 vs. a^2/d^2 with an ideally conducting wall. Shown are the results for the three shapes (inverse dee, ellipse, regular dee) at high β_p (solid symbols) and low β_p (open symbols).

Fig. 6. Plot of γ^2 vs. a^2/d^2 with an ideally conducting wall for DIII-D-like equilibria with no pressure and $l_i = 0.6$ (dashed curve) and $l_i = 0.8$ (solid curve).

Fig. 7. Growth rates (in s^{-1}) vs. l_i for a configuration that is stabilized by discrete conductors with the vacuum vessel far from the plasma. For comparison are shown growth rates with a completely surrounding wall (conformal to the plasma surface at $d = 1.3a$).

Fig. 8. The plasma boundary, the discrete conductor sets, and perturbed flux contours are shown for the high l_i and low l_i cases in the configuration with discrete conductors. The vacuum vessel is quite distant from the plasma. Also shown as a dashed contour is the fictitious wall used for comparison in Fig. 7.

Figure 1

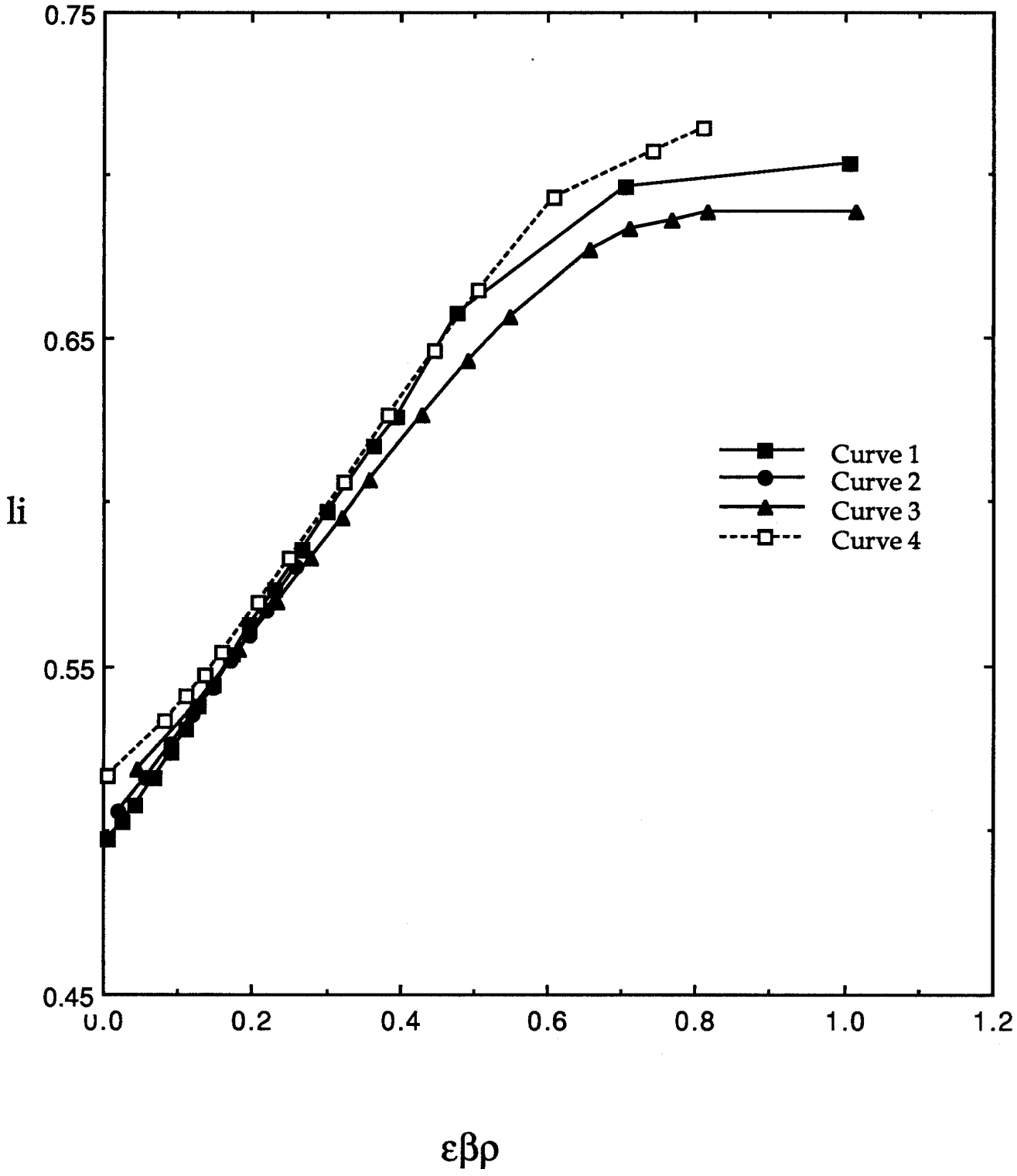
0.75
0.65
0.55
0.45
li
0.0
0.2
0.4
0.6
0.8
1.0
1.2
εβρ
Curve 1
Curve 2
Curve 3
Curve 4

Figure 2

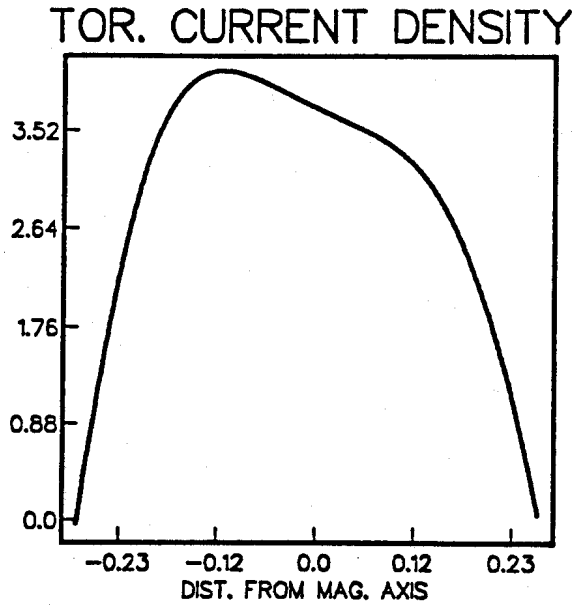

(a)

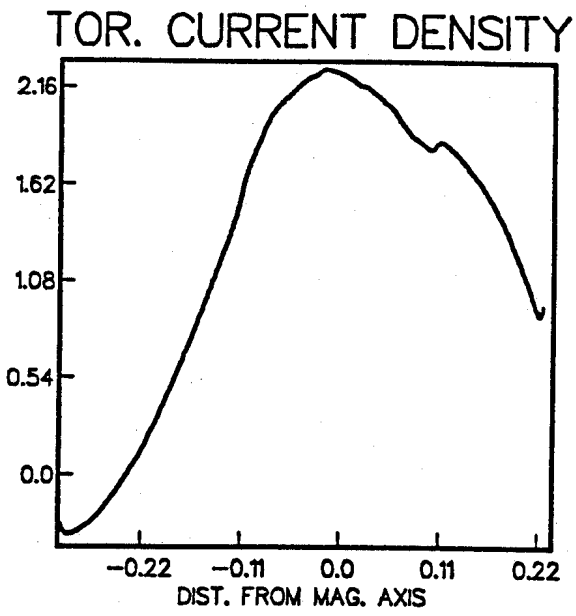

(b)

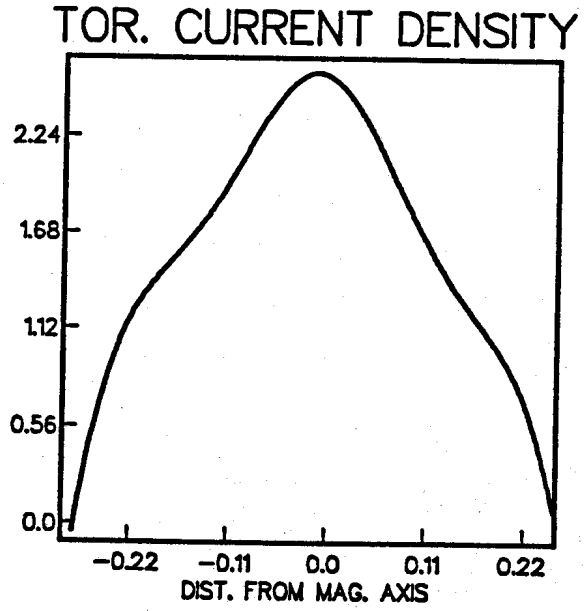

(c)

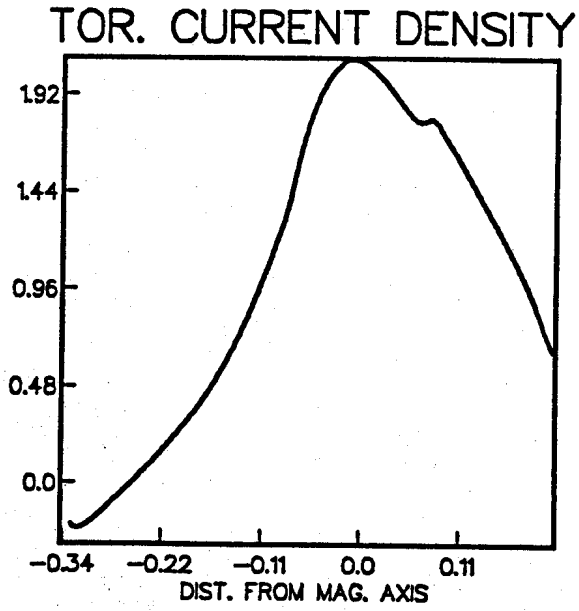

(d)

Figure 3

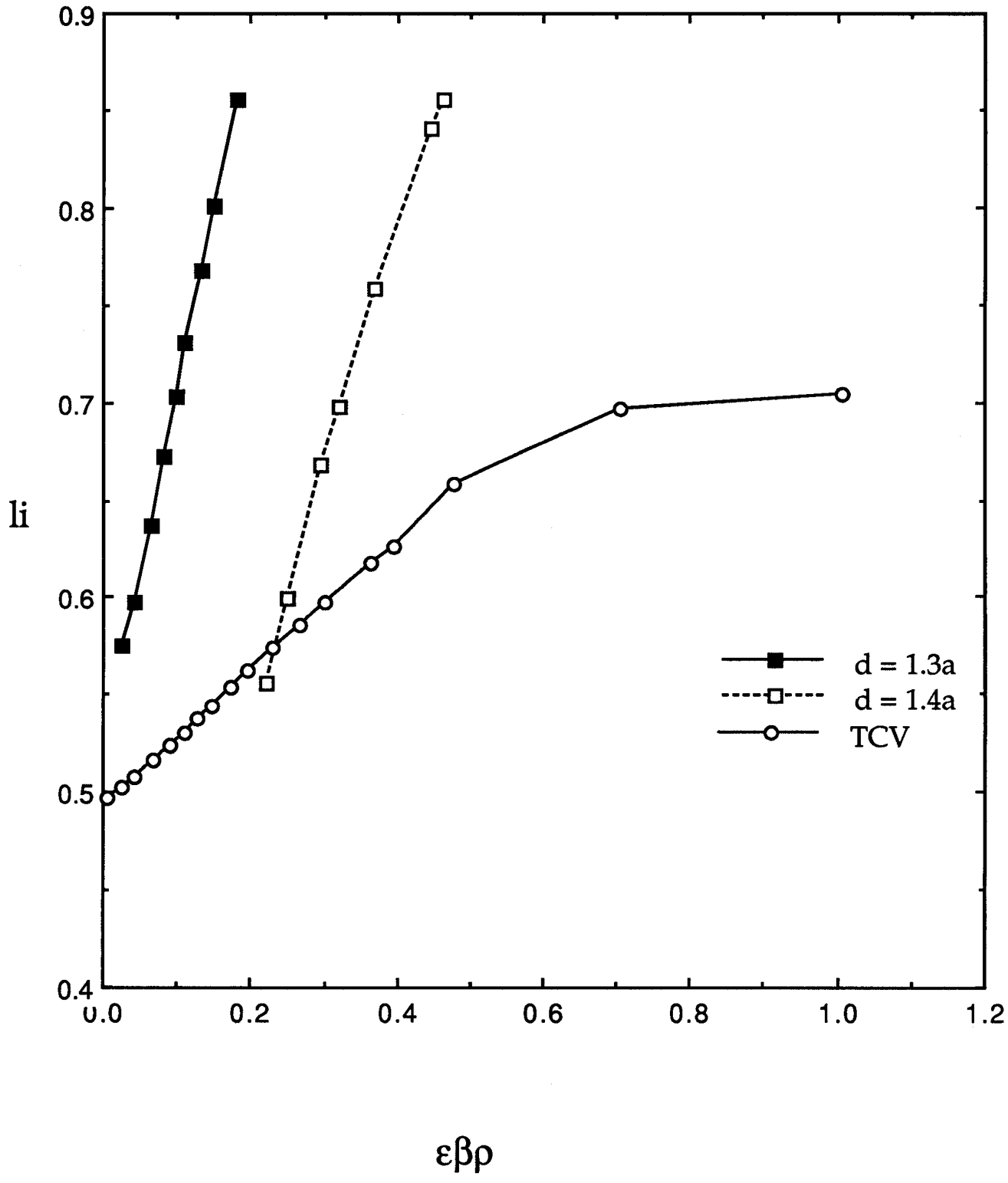

Figure 4

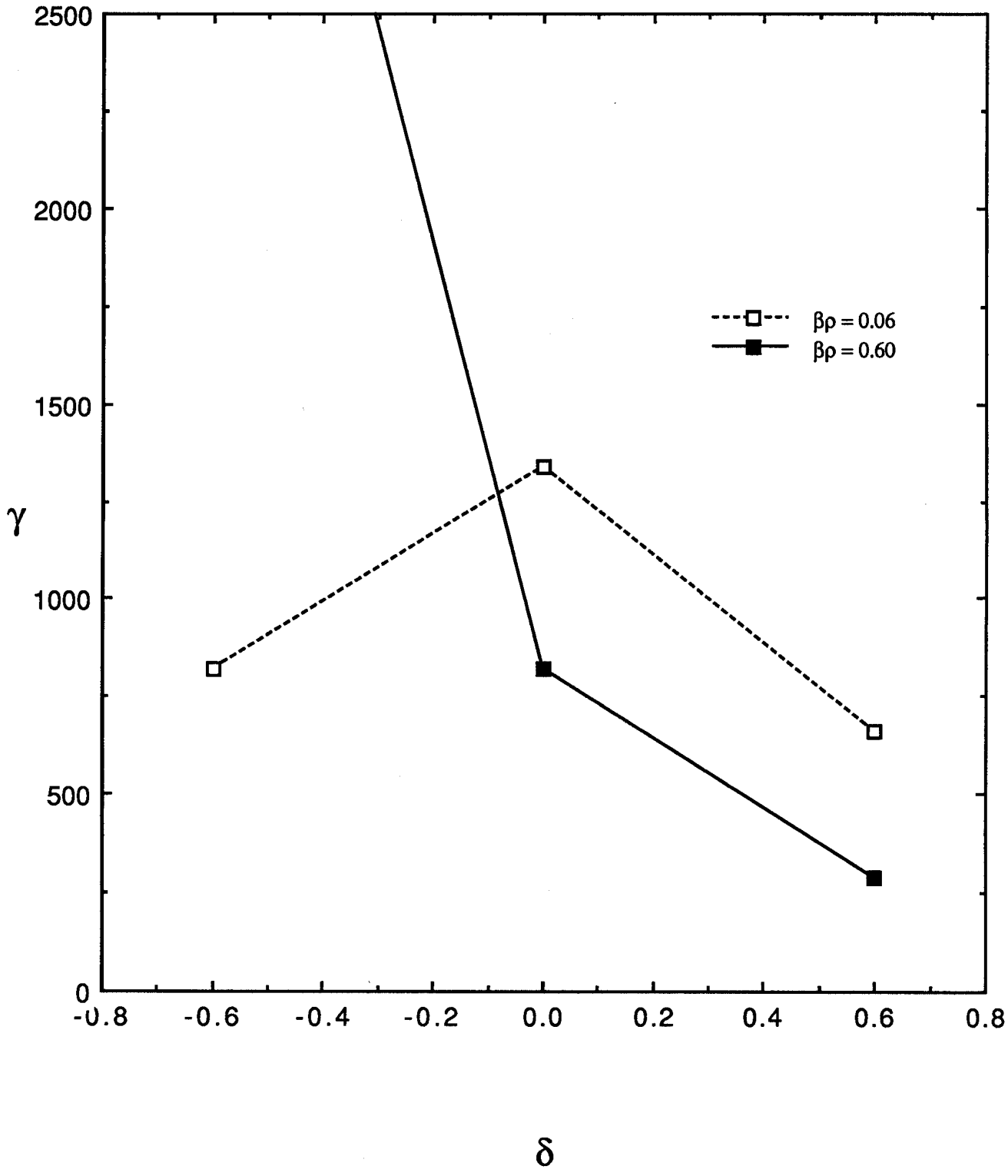
2500
2000
1500
1000
500
0
γ
-0.8
-0.6
-0.4
-0.2
0.0
0.2
0.4
0.6
0.8
δ
βρ = 0.06
βρ = 0.60

Figure 5

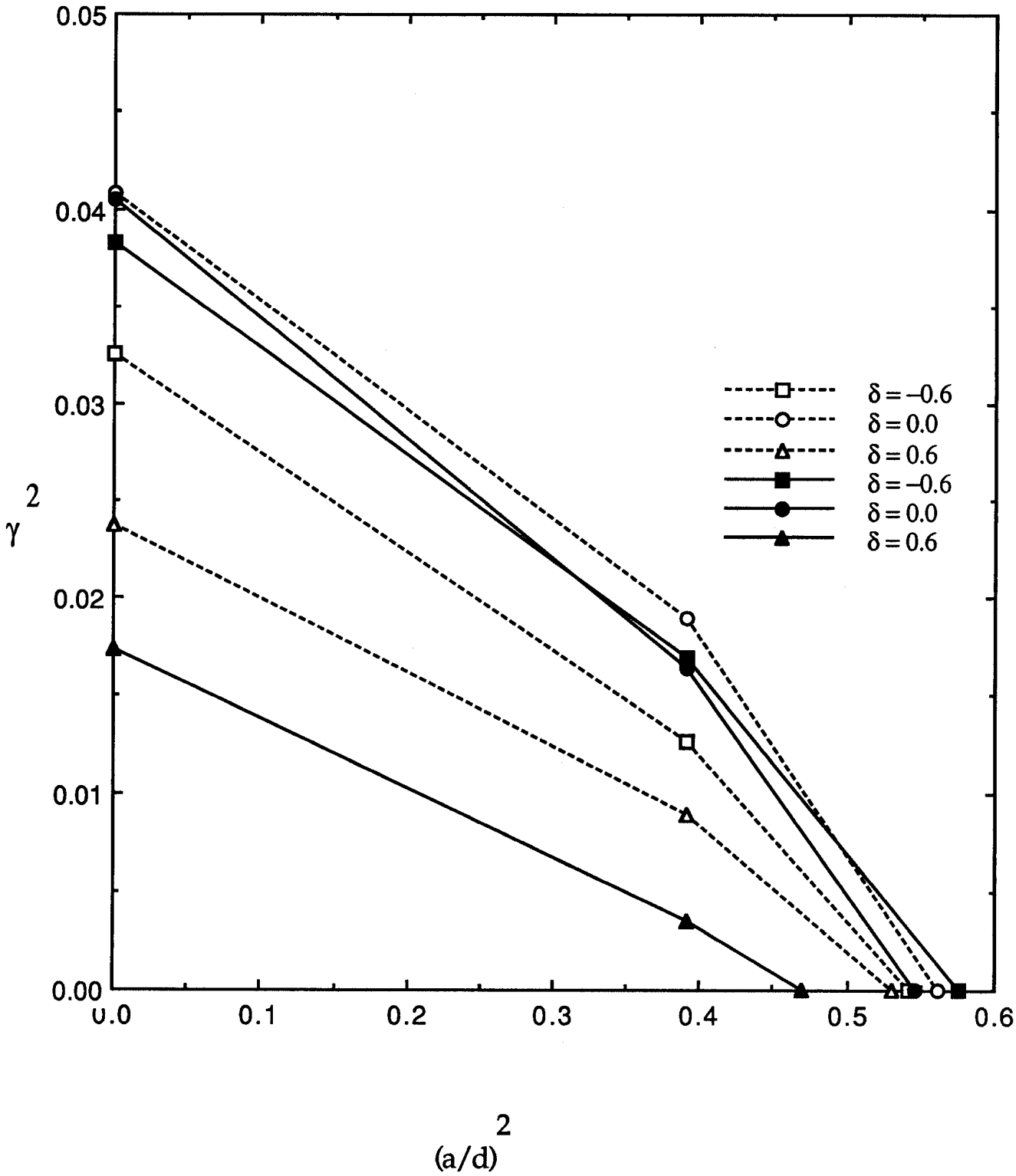
0.05
0.04
0.03
0.02
0.01
0.00
0.0
0.1
0.2
0.3
0.4
0.5
0.6
γ 2
(a/d) 2
δ = –0.6
δ = 0.0
δ = 0.6
δ = –0.6
δ = 0.0
δ = 0.6

Figure 6

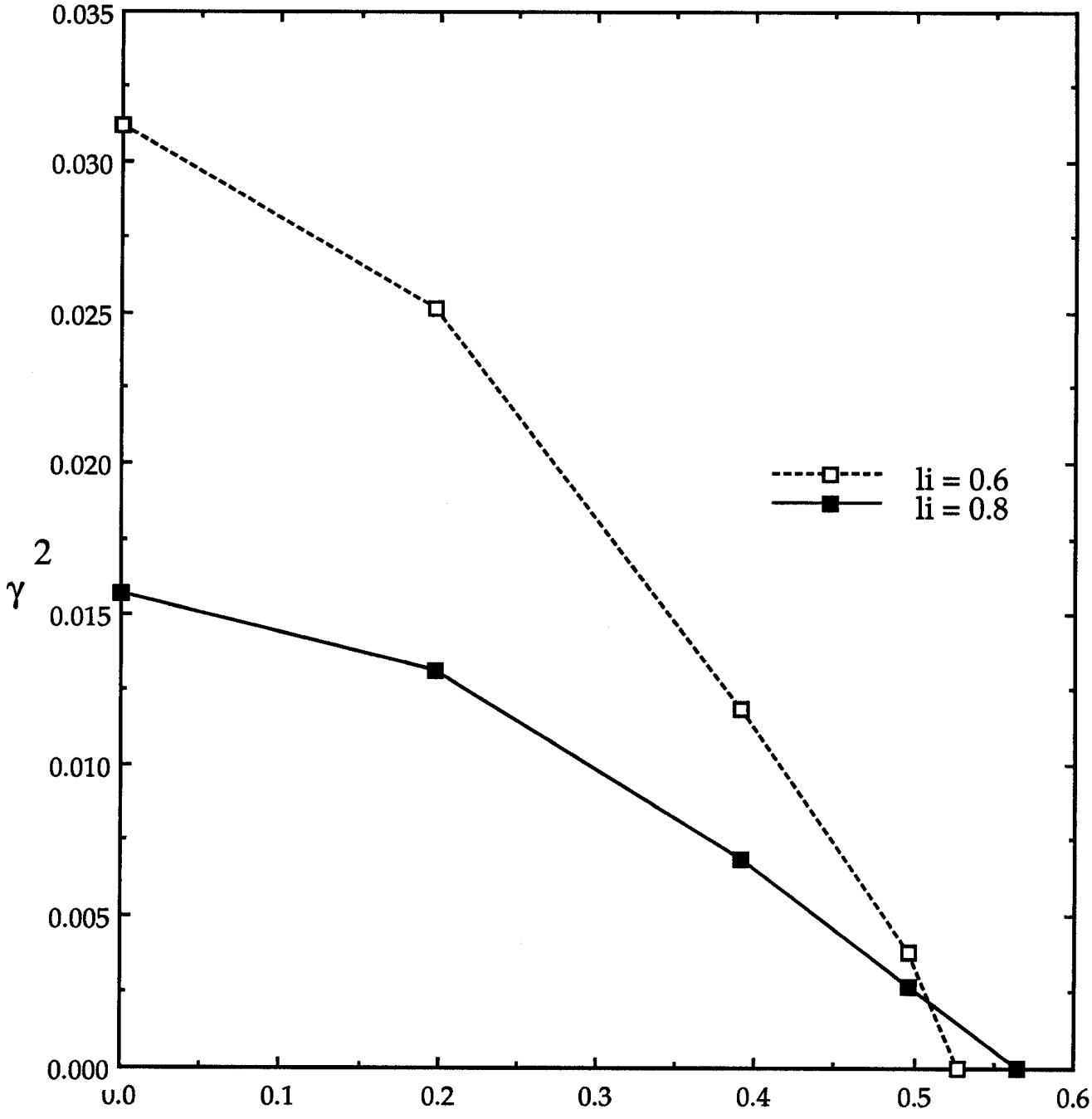
0.035
0.030
0.025
0.020
0.015
0.010
0.005
0.000
γ 2
0.0
0.1
0.2
0.3
0.4
0.5
0.6
li = 0.6
li = 0.8
2
(a/d)

Figure 7

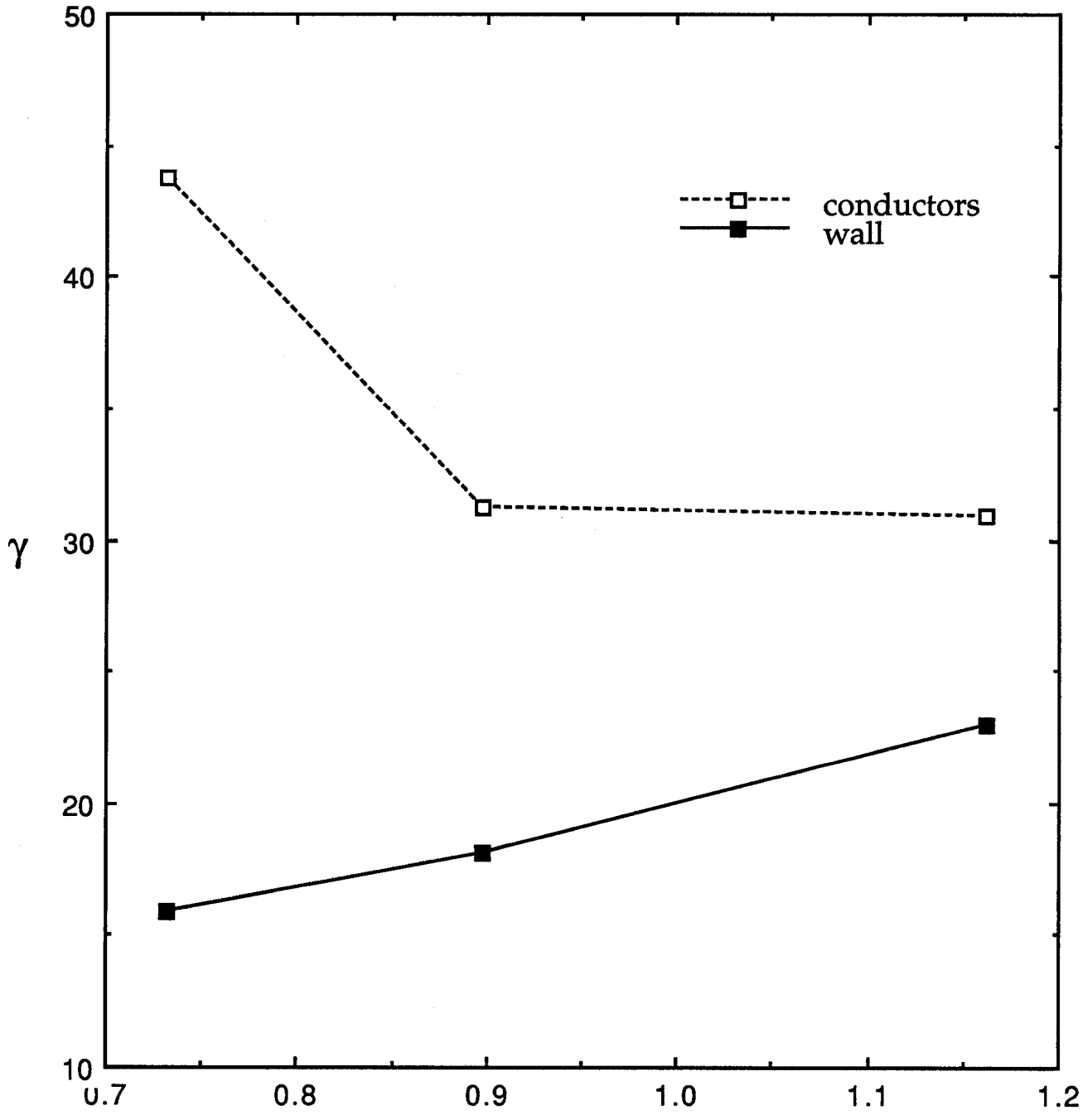

Figure 8 (a)

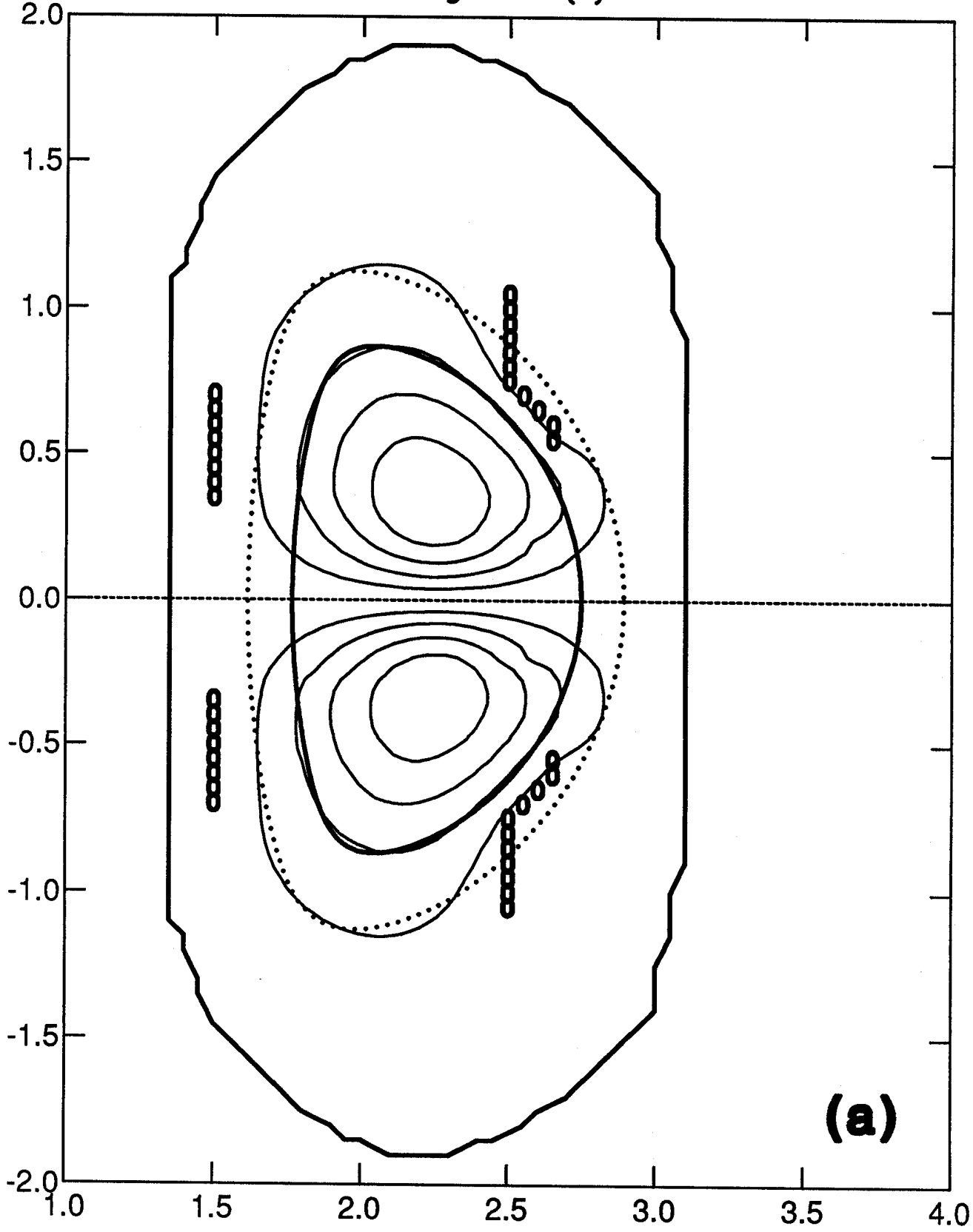

Figure 8 (b)